coatings

MDPI

Article

# Enhanced Corrosion Protection of Iron by Poly(3-hexylthiophene)/Poly (styrene-*co*-hydroxystyrene) Blends

**Ming-Chia Tsai, Chung-Ru Yang, Jen-Hao Tsai, Yuan-Hsiang Yu * and Ping-Tsung Huang ***

Department of Chemistry, Fu Jen Catholic University, Hsinchuang Dist., New Taipei City 24205, Taiwan; p22608352@hotmail.com (M.-C.T.); A0922430809@gmail.com (C.-R.Y.); ahahacao@gmail.com (J.-H.T.)

* Correspondence: 084916@mail.fju.edu.tw (Y.-H.Y.); 073802@mail.fju.edu.tw (P.-T.H.); Tel.: +886-2-29052476 (P.-T.H.)

Received: 18 September 2018; Accepted: 25 October 2018; Published: 27 October 2018

**Abstract:** Corrosion of iron in NaCl solution is significantly reduced by poly(3-hexylthiophene) (P3HT)/poly(styrene-*co*-hydroxystyrene)(PS-*co*-PHS) blended coating layers, especially at elevated temperature. The interaction between sulfur (in P3HT) and hydroxyl group (in PS-*co*-PHS) leads to enhanced miscibility between P3HT and PS-*co*-PHS and results in improved thermal stability upon thermal treatment. Adhesion force between iron and the coating layer is increased with increasing hydroxystyrene ratio as revealing by the adhesion test (ASTM 3359). Anticorrosion properties from electrochemical experiments indicate great improvement over the P3HT/PS blend. Protection efficiency (PE) of P3HT/PS-*co*-PHS blend on iron increases and corrosion rate (mils per year, MPY) decreases upon thermal treatment, making P3HT/PS-*co*-PHS blend an excellent corrosion inhibitor and adhesion promoter material to the iron, especially with good thermal stability.

**Keywords:** P3HT; PS; PHS; miscibility; anticorrosion; stability

## 1. Introduction

Corrosion of metal has been a serious problem in our daily life. It causes billions of dollars of economic losses every year [1]. In order to diminish the damage caused by corrosion, scientists have conducted many experiments to lessen the risk of corrosion on metals such as cathodic, anodic and adsorption protection [2]. A lot of research effort has focused upon the development of advanced organic coating materials as corrosion barriers (or corrosion inhibitors) in the last few decades [2–6] and much improvement has been observed on different metals. Generally speaking, the application of organic coatings as anticorrosion materials can be divided into the following categories. The first category is the usage of gas permeation membranes to lower the oxygen and moisture penetration rate and retard the occurrence of a corrosion reaction [7–13]. The most commonly used materials are polymer blends containing layered materials such as montmorillonite (MMT) and reduced graphene oxide (RGO). Intercalated MMT or RGO in polymers decrease the gas and moisture penetration rate because their high aspect ratio and layer structure, which lowers the corrosion rate. The second category is the introduction of specific interaction from the organic coating layer to metal to enhance bonding between organic coating and metal [5,14–16]. This prevents penetration of corrosive materials to the surface of metal and gives rise to higher anticorrosion stability. The last category is the application of conjugated polymers to corrosion protection on metals [6,17]. Conjugated polymers induce passivation layers on top of metals so that metal oxide interlayers between conjugated polymers and metals form and protect the metal from corrosion reaction. MacDiarmid [18] applied polyaniline (PANI) on top of stainless steel and found the formation of a passivation layer between the stainless steel

and PANI. Epstein [19] showed the formation of $Fe_3O_2$ and $Fe_3O_4$ at the interface of emeraldine base PANI and iron by coating an emeraldine base polyaniline on top of iron. Both have demonstrated the anticorrosion effect of conjugated polymers on metals.

Although conjugated polymers can act as corrosion barriers, penetration of corrosive anions (such as $Cl^-$) through the free volume within polymers and the interface between conjugated polymers and metals can also still deteriorate the metal [5]. Therefore, an effective approach that can simultaneously prevent the moisture penetration through the conjugated polymers and enhance the bonding between anticorrosion coating layer and metal becomes very important.

Among all different kinds of conjugated polymers for anticorrosion study, PANI has been commonly selected as the model polymer because of its ease of preparation and also its good anticorrosion properties after suitable modification with other materials [18–22]. However, PANI tends to absorb moisture easily because of its amine nature and this leads to a long-term stability issue. Researchers found conjugated polymers containing sulfur such as poly(3-alkylthiophenes) (P3AT) exhibit excellent anticorrosion properties on metals [23–27]. Generally, the corrosion protection efficiency (PE) of polythiophenes on metals are over 90%. Guo [23] uses the DFT calculation to study this empirical rule and finds the electron donating ability and the energy of the $\pi$ molecular orbital are related to this adsorption behavior. Although P3ATs are with good anticorrosion properties, they are expensive and have poor mechanical properties [27]. Therefore, an efficient preparation of P3AT composites to cost down and also to further enhance anticorrosion properties, especially at elevated temperature becomes very important. Blends of P3HT with polystyrene (PS) or poly(methyl methacrylate) (PMMA) have been used to study the anticorrosion phenomenon on steel. Experimental results demonstrate improved anticorrosion properties at 100 °C [26,27]. However, anticorrosion properties start to deteriorate at elevated temperature because of the cracking of the blends. It seems that phase separation plays an important role in this consequence. Yong [22] studies the corrosion inhibiting behavior of epoxidized natural rubber blends on carbon steel and finds extent of phase separation between epoxy and natural rubber components are correlated to the anticorrosion efficiency. Higher compatibility polymer composites usually give rise to better anticorrosion efficiency. Schauer [20] studies the corrosion behavior of PANI/epoxy on iron using Iron/PANI/epoxy layered structure and finds that phase separation between PANI and epoxy layer ending up with intercoat delamination that lowers the protection efficiency of the organic coating on iron. In order to achieve stronger bonding between the organic coatings and metals, researchers have synthesized coating materials with different functionalities such as phosphoric acid [14,15], hydroxyl group [16], and polyionic liquid [5]. Interfacial bonding between the organic coating layer and the metal is, therefore, increased and anticorrosion property is improved.

From the literature study, it becomes very crucial that an organic coating with the following properties can act as corrosion inhibitor layer on metals: low moisture penetration; good adsorption to the metal surface; quick metal oxide formation as passivation layer.

In this work, P3HT is chosen as the key corrosion inhibitor to protect iron from corrosion. To minimize usage of P3HT and increase bonding strength between P3HT and the iron substrate, PS-*co*-PHS copolymers with different hydroxystyrene contents are synthesized. Hydroxyl group in copolymer can further enhance bonding between P3HT/PS-*co*-PHS blends. The hydroxyl group interacts with sulfur atom in P3HT and enhances the compatibility between P3HT and PS-*co*-PHS copolymers, which may also improve the thermal stability of these coating blends.

## 2. Materials and Methods

### 2.1. Materials

All chemicals except styrene and Azobisisobutyronitrile (AIBN) were used without further purification. Styrene was purified by distillation under reduced pressure from commercial styrene (ACROS Co., Morris Plains, NJ, USA). AIBN was purified by recrystallization from methanol (98%,

TCI Co., Taipei, Taiwan). 1,4-Dioxane (spectrum grade) was purchased from Tedia Co. (Fairfield, OH, USA). Hydrazine monohydrate and 4-acetoxystyrene were purchased from ACROS Co. Polystyrene (PS, $\overline{M_n}$ = 155,000) was purchased from Scientific Polymer Products Inc. (Ontario, NY, USA). o-Xylene was purchased from Grand Chemicals Co. (Mysore, India). P3HT ($\overline{M_n}$ =25,700, $\overline{M_w}$ = 50,100, Regioregularity = 97%) was purchased from Rieke Metals Inc. (Lincoln, NE, USA).

#### 2.1.1. Synthesis of Poly(styrene-*co*-acetoxystyrene)

Both 5% and 10% acetoxystyrene and styrene copolymers, poly(styrene-*co*-acetoxystyrene)(PS-*co*-5PAS and PS-*co*-10PAS), were synthesized in the same procedures except for a difference in the styrene and acetoxystyrene ratio. AIBN (20 mg), 4-acetoxystyrene (0.5 g; 1.32 g) and styrene (9.32 g; 8.7 g) were added to a round-bottomed flask containing 1,4-dioxane (16 mL) and reacted at 80 °C for 72 h. After cooling to room temperature, it was diluted with 100 mL toluene and precipitated into methanol many times. The copolymer was dried under reduced pressure at 50 °C. PS-*co*-5PAS (7.8 g, 79%) and PS-*co*-10PAS (8.0 g, 80%) were collected.

#### 2.1.2. Synthesis of Poly(styrene-*co*-hydroxystyrene)

PS-*co*-5PAS (1.6 g) (or PS-*co*-10PAS) and hydrazine hydrate (3 mL) were dissolved in 1,4-dioxane (27 mL) in a round-bottomed flask. The mixture was reacted for 12 h at room temperature under $N_{2(g)}$ and was precipitated into methanol and then filtrated. The polymers were reprecipitated twice from methanol. After filtered, the residue was washed by methanol and dried under reduced pressure. PS-*co*-5PHS (1.28 g, 80%) and PS-*co*-10PHS (1.25 g, 78%) were collected.

### *2.2. Polymer Characterization*

1H NMR (300 MHz) spectra were recorded overnight (more than 10 h) on a Bruker AC-300 MHz (Bruker Corp., Billerica, MA, USA). Molecular weight of polymers was measured by a Viscotek DM400/LR40 (Malvern Panalytical, Malvern, UK) Gel Permeation Chromatography (GPC) using standard polystyrene as reference.

### *2.3. Optical Microscopy Measurement*

Optical microscope photos were taken using an Olympus BH-2 Microscopy with a 40× object lens (Olympus, Tokyo, Japan). Glass substrates are cleaned in an ultrasonic bath using detergent, deionized water, acetone, and isopropanol sequentially. Solutions of P3HT blended with PS or PS-*co*-PHS (PS-*co*-5PHS and PS-*co*-10PHS) at 1:1 ratio in o-xylene were spin-coated on glass using a Conch Corp. spin-coater (Conch Corp., Taipei, Taiwan) at 500 rpm for 50 s and 1000 rpm for 100 s. They were dried at 25, 100 and 200 °C for 1 h in air before measurement.

### *2.4. Corrosion Test*

Electrochemical measurements were conducted on a CHI 680C Cyclic Voltammetry (CH Instruments, Austin, TX, USA). Iron substrates were ground with 150, 400, 600 and 800 grade sandpapers before coating. Iron substrates are cleaned in ultrasonic bath with hexanes after grinding. Polymer solutions in *o*-xylene were spin-coated onto iron substrate and dried at 25, 100, and 200 °C for one hour before measurement. The thickness measurement is conducted with an Elcometer type 456 gauge meter (Elcometer Co., Manchester, UK). The contact angle is measured with a FACE contact angle meter model XP1502 (Tantec Inc., Schaumburg, IL, USA). All corrosion tests are performed in a 3.5% NaCl solution (food grade) and all samples are immersed in a corrosive medium for 30 min.

## 3. Results and Discussion

Experimental procedures for the synthesis of PS-*co*-5PHS and PS-*co*-10PHS are outlined in Scheme 1 and physical properties are listed in Table 1.

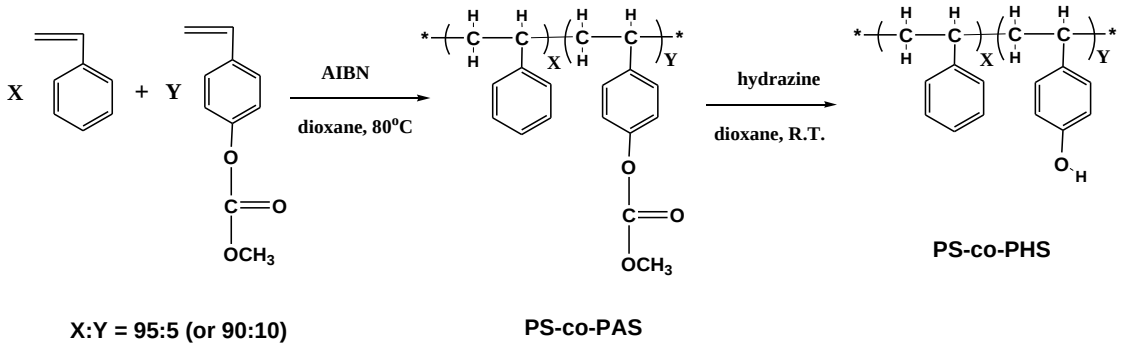


**Scheme 1.** Synthetic routes of the PS-*co*-5PHS and PS-*co*-10PHS.

**Table 1.** Physical properties of PS, PS-*co*-5PHS, and PS-*co*-10PHS.

| Polymer | $\overline{M_n}$ (*Da*) | $\overline{M_w}$ (*Da*) | PDI | $T_d$ (°C) | $T_g$ (°C) |
|---|---|---|---|---|---|
| PS | 155k | 253k | 1.6 | 417.6 | 101.9 |
| PS-*co*-5PHS | 185k | 273k | 1.5 | 384.8 | 104.7 |
| PS-*co*-10PHS | 121k | 203k | 1.7 | 373.8 | 109.1 |

$\overline{M_n}$: number average molecular weight; $\overline{M_w}$: weight average molecular weight; PDI: polydispersity index = $\overline{M_w}/\overline{M_n}$; $T_d$: decomposition temperature; $T_g$: glass transition temperature.

Characteristic peak of acetyl group appears at 2.27 ppm (Figure 1) in NMR measurement shows the successful synthesis of PS-*co*-PAS copolymers. Molar ratio of styrene to acetoxystyrene in PS-*co*-5PAS and PS-*co*-10PAS are calculated by peak area from NMR spectra and the ratio are around 95:5 and 90:10, respectively. After reaction with hydrazine, characteristic peak of acetyl group disappears and a broad peak representing the hydroxyl group shows up at 4.45 ppm indicating successful synthesis of PS-*co*-5PHS and PS-*co*-10PHS.

To investigate the intermolecular interaction between P3HT and PS-*co*-PHS, p-cresol and 3-hexylthiophene are used as model compounds in this study. An illustration of the molecular interaction is shown in Figure 2.

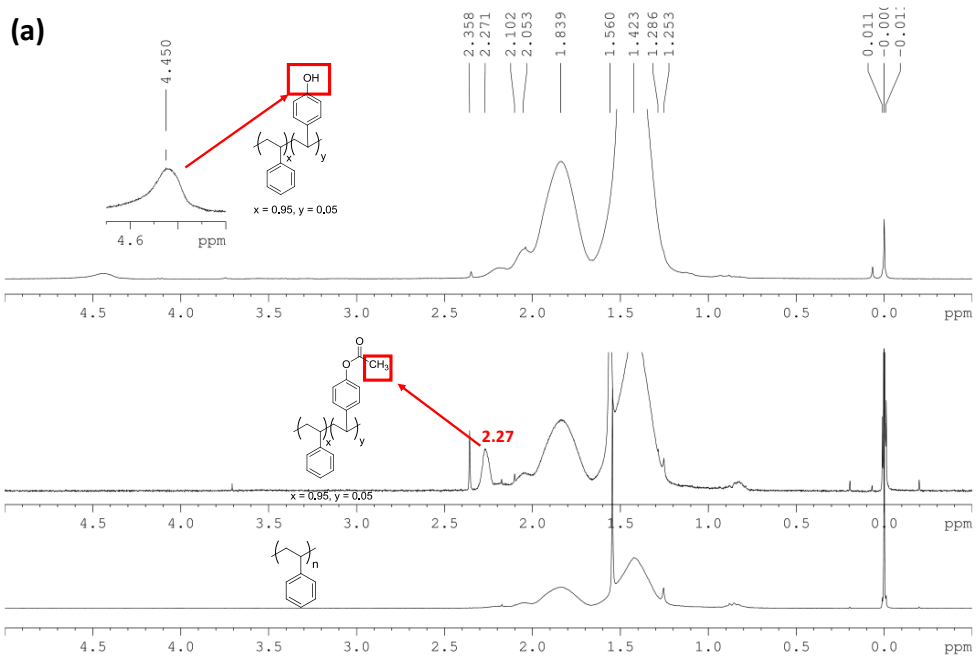


**Figure 1.** *Cont.*

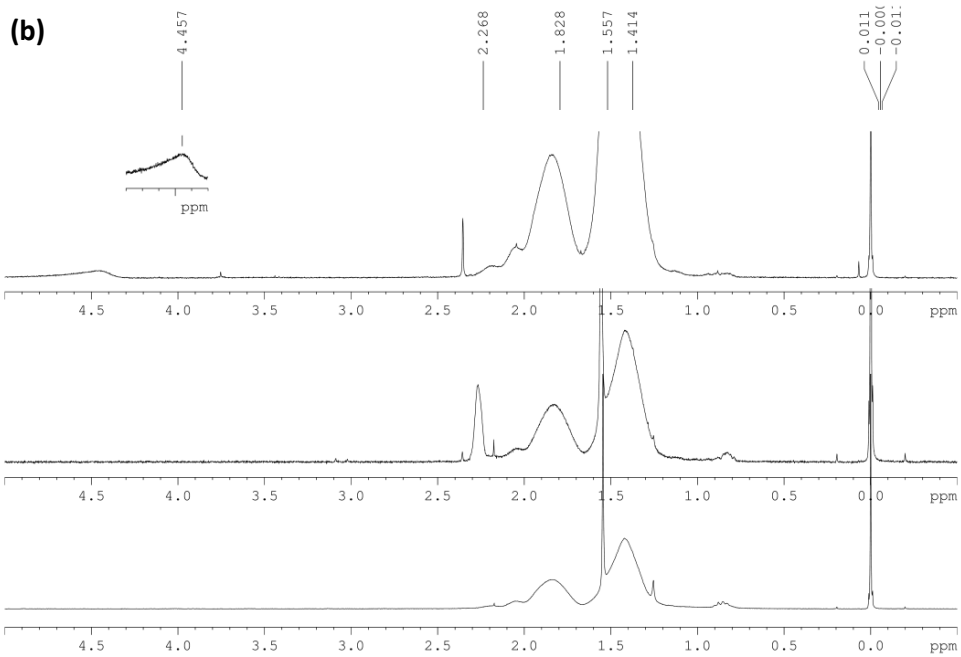


**Figure 1.** NMR spectra of (**a**) PS/PS-co-5PAS/PS-co-5PHS and (**b**) PS/PS-co-10PAS/PS-co-10PHS.

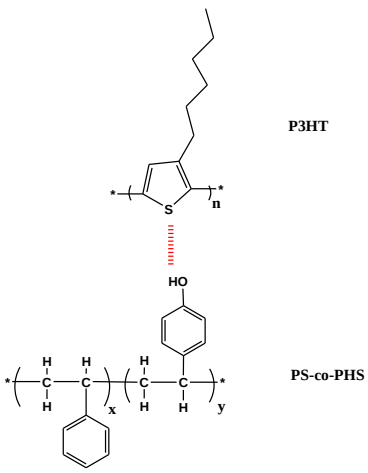


**Figure 2.** Illustration of molecular interaction between P3HT and PS-*co*-PHS.

As shown in Figure 3a, a broad peak between 3.8 and 4.8 ppm (Figure 3a, top) representing the hydrogen-bonding of the hydroxyl group of p-cresol becomes a sharp peak at 4.68 ppm. This result indicates the intermolecular interaction between S atom of the 3-hexylthiophene and the hydroxyl group of the p-cresol restricting the motion of hydroxyl group. The wave number of the hydroxyl group in p-cresol gradually shifts from 3281 to 3542 $cm^{-1}$ as the ratio of 3HT increases in the 3HT/p-cresol blend indicating the increased interaction between hydroxyl group and thiophene unit. This molecular interaction has a profound effect on the compatibility improvement between PS and P3HT (Figure 4). P3HT and PS do not have a strong molecular interaction and result in severe phase separation after the spin-coating process, even at room temperature. As the interaction force between P3HT and PS increases by the introduction of hydroxyl group to the PS, compatibility was significantly enhanced. By incorporation of 5% hydroxyl group to PS (PS-*co*-5PHS), compatibility between PS and P3HT has already improved a great deal. However, phase separation appears gradually at elevated temperature. By incorporation of 10% hydroxyl group to the PS (PS-*co*-10PHS), thermal stability of the blend is greatly improved. Only a minor phase separation occurs at 200 °C.

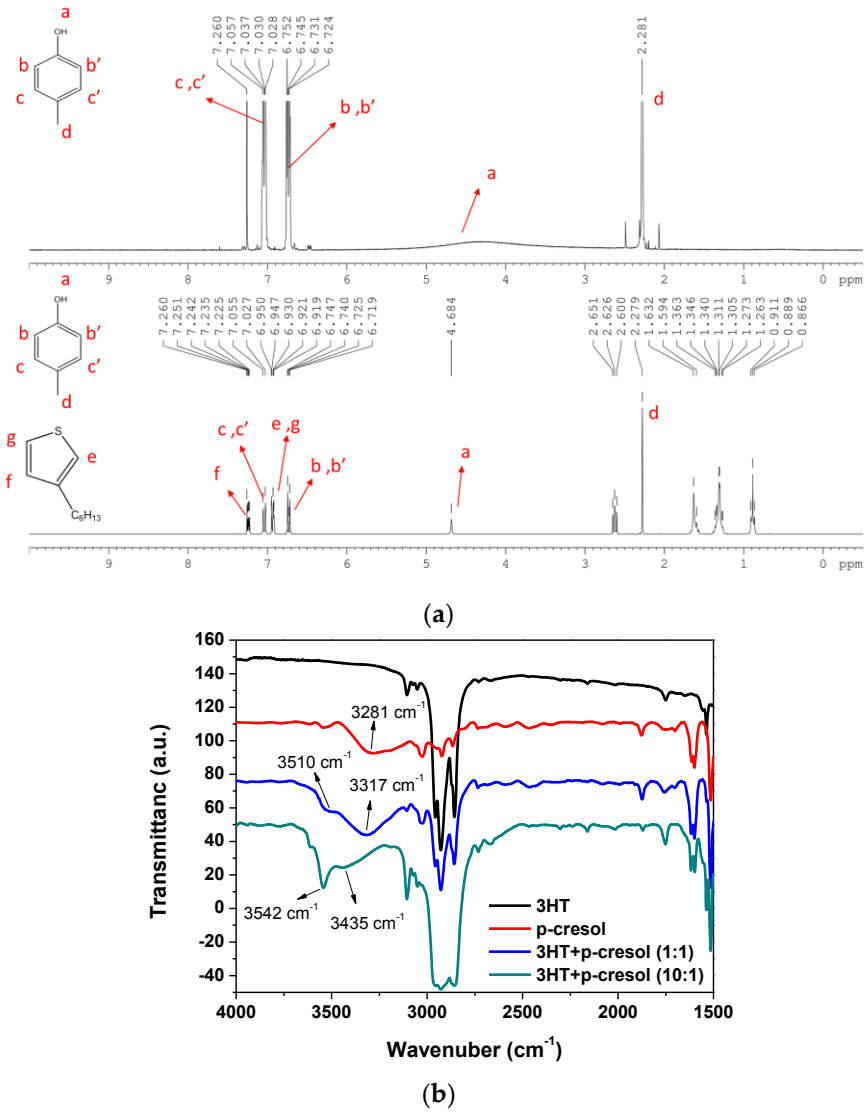


**Figure 3.** (**a**) NMR spectra of p-cresol and p-cresol/3-hexylthiophene (3HT) (1:1); (**b**) FT-IR spectra of 3HT, p-cresol, and 3HT/p-cresol blends (1:1 and 10:1).

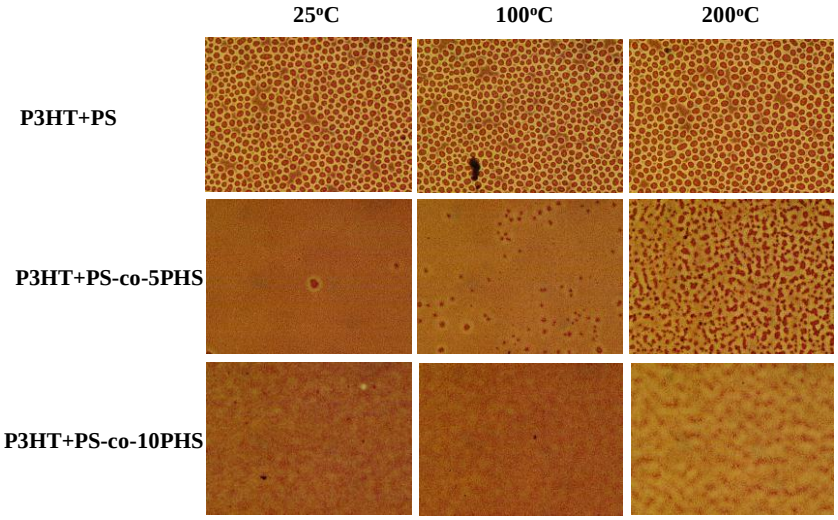


**Figure 4.** Optical microscope photos of P3HT + PS (1:1), P3HT + PS-*co*-5PHS (1:1) and P3HT + PS-*co*-10PHS blends after spin-coating on glass and annealed at 25, 100 and 200 °C.

Incorporation of hydroxyl group to the PS not only improves compatibility and thermal stability of the P3HT/PS blends, but also increases the bonding strength between P3HT/PS blend and the iron substrate (Figure S1). As shown in Table 2, P3HT shows poor adhesion to the iron and fails in the adhesion test. Poor adhesion to the substrate allows corrosive materials such as $Cl^-$ ion to penetrate to the interface or surface of substrate and deteriorate the interface. For P3HT/PS blends, all samples fail in the adhesion test no matter whether they are thermally treated or not. As hydroxyl group is incorporated into PS, adhesion force is significantly improved. Both P3HT/PS-*co*-5PHS and P3HT/PS-*co*-10PHS show no coating materials transferring to the tape at room temperature (25 °C). The PS-*co*-PHS acts as primer to enhance the bonding strength of P3HT to the iron. Adhesion test of the high temperature (100 and 200 °C) treated samples also show no polymers transferring to the tape, indicating good bonding strength of the P3HT/PS-*co*-PHS blends to the iron after thermal treatment.

**Table 2.** Adhesion tests (ASTM 3359) and contact angle measurements of water on P3HT and its blends at room temperature (25 °C), 100 °C, and 200 °C treatment.

| Coating Layer | 100 Grid Test | Contact Angle (°) |
|---|---|---|
| P3HT, 25 °C | 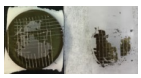 | 100.6 |
| P3HT + PS, 25 °C |  | 98.9 |
| (P3HT + PS), 100 °C | 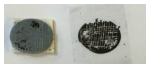 | 101.0 |
| (P3HT + PS), 200 °C |  | 98.4 |
| P3HT + PS-*co*-5PHS, 25 °C |  | 102.6 |
| P3HT + PS-*co*-5PHS, 100 °C |  | 102.6 |
| P3HT + PS-*co*-5PHS, 200 °C |  | 98.6 |
| P3HT + PS-*co*-10PHS, 25 °C |  | 104.5 |
| P3HT + PS-*co*-10PHS, 100 °C |  | 102.9 |
| P3HT + PS-*co*-10PHS, 200 °C |  | 99.4 |

The enhanced bonding between the organic coating layer and iron surface leads to significant effect on the anticorrosion behavior of the P3HT/PS-*co*-PHS blends. As seen in Figure 5, the $I_{corr}$ of P3HT/PS blend increases at elevated thermal treatment temperature. $I_{corr}$ increases from 0.71 μA/cm$^2$ at 25 °C to 9.40 μA/cm$^2$ at 200 °C (Table 3) indicating corrosion protection of the polymer blend coating layer to the iron surface is getting worse at elevated temperature. However, $I_{corr}$ decreases as content of hydroxyl group increases in the PS-*co*-PHS copolymers. $I_{corr}$ decreases from 0.71 μA/cm$^2$ for the P3HT/PS to 0.25 μA/cm$^2$ for the P3HT/PS-*co*-10PHS at 25 °C. These data match the results shown in the adhesion test. The bonding strength of the P3HT/PS blend does increase with the incorporation of hydroxyl group. As mentioned above, P3HT/PS blend does not have good bonding to the iron surface so protection efficiency (PE) decreases dramatically after thermal treatment (Table 3). However, both P3HT/PS-*co*-5PHS and P3HT/PS-co-10PHS show very consistent anticorrosion properties at elevated temperature because of the improved adhesion force and thermal stability. $I_{corr}$ are both decreased for these two hydroxyl groups containing blends at elevated temperature. For the P3HT/PS-*co*-5PHS sample, it decreases from 0.41 μA/cm$^2$ for untreated sample (25 °C) to 0.13 μA/cm$^2$ for the 200 °C treated one. For the P3HT/PS-co-10PHS sample, $I_{corr}$ decreases from 0.25 μA/cm$^2$ for untreated

sample (25 °C) to 0.04 μA/cm$^2$ for the 200 °C treated sample. $R_{corr}$ (MPY) shows similar trend to the $I_{corr}$ and PE value are all above 96%. $R_p$ decreases at elevated temperature for the P3HT/PS blend, but these values increase after thermal treatment for the P3HT/PS-*co*-PHS blends, indicating enhanced protection efficiency of the PS-*co*-PHS blends to the iron substrate and lowing the corrosion rate (MPY).

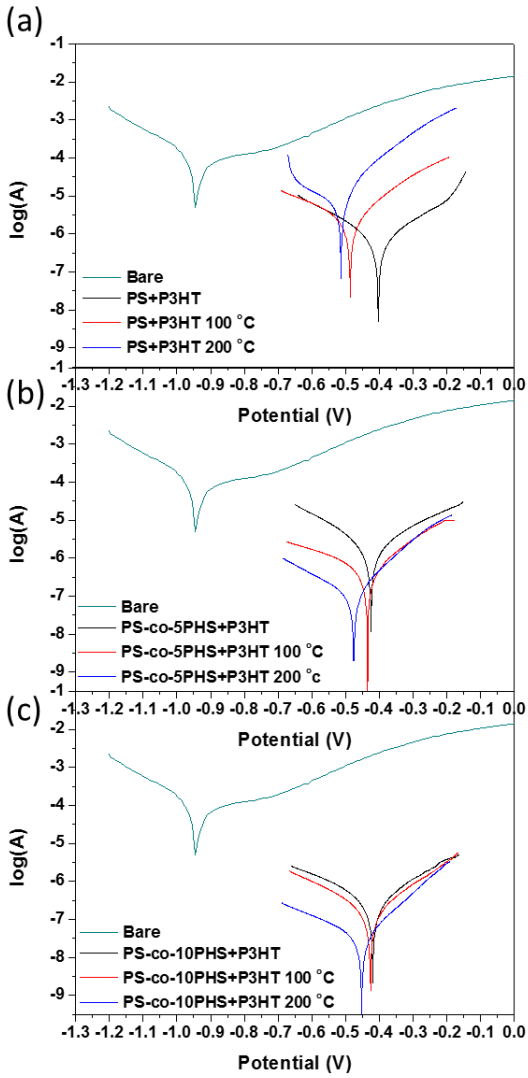


**Figure 5.** Tafel plots of (**a**) P3HT/PS, (**b**) P3HT/PS-*co*-5PHS and (**c**) P3HT/PS-*co*-10PHS at 25, 100, and 200 °C.

**Table 3.** Electrochemical properties of P3HT + PS, P3HT + PS-*co*-5PHS, and P3HT + PS-*co*-10PHS coated iron substrates in 3.5% NaCl solution.

| Coating Layer [a] | $R_p$ (kΩ cm$^2$) | $I_{corr}$ (μA/cm$^{-2}$) | $R_{corr}$ (MPY [c]) | PE [b] (%) | Thickness (μm) |
|---|---|---|---|---|---|
| bare-Fe | 4.20 | −15.38 | 7.02 | – | – |
| P3HT, 25 °C | 44.1 | −1.03 | 0.47 | 97.8 | 10.0 |
| P3HT + PS, 25 °C | 51.2 | −0.71 | 0.32 | 95.4 | 8.47 |
| (P3HT + PS), 100 °C | 15.0 | −2.37 | 1.08 | 84.6 | 9.52 |
| (P3HT + PS), 200 °C | 2.20 | −9.40 | 4.30 | 38.9 | 5.10 |
| P3HT + PS-*co*-5PHS, 25 °C | 100 | −0.41 | 0.19 | 97.3 | 12.04 |
| P3HT + PS-*co*-5PHS, 100 °C | 321 | −0.48 | 0.22 | 96.8 | 16.30 |
| P3HT + PS-*co*-5PHS, 200 °C | 249 | −0.13 | 0.06 | 99.1 | 16.70 |
| P3HT + PS-*co*-10PHS, 25 °C | 1357 | −0.25 | 0.11 | 98.4 | 13.63 |
| P3HT + PS-*co*-10PHS, 100 °C | 2275 | −0.16 | 0.07 | 99.0 | 13.98 |
| P3HT + PS-*co*-10PHS, 200 °C | 926 | −0.04 | 0.02 | 99.7 | 10.89 |

[a]: blend ratio is 1:1; [b]: corrosion protection efficiency; [c]: mils per year (corrosion rate).

Electrochemical impedance spectroscopy (EIS) results of the above samples are shown in Figure 6. The charge transfer resistance ($R_{ct}$, radius of the semi-circle) of the polymer coated iron substrate in 3.5% NaCl solution increases with incorporation of hydroxyl group to the PS. Additionally, all thermally treated samples have a higher charge transfer resistance than those without thermal treatment. The inconsistency in the straight line region during the measurement may attributed to the compatibility variation for the P3HT/PS and P3HT/Ps-*co*-PHS blends, especially at elevated temperature. Polymer blends tend to phase separate upon thermal treatment depending on the strength of intermolecular force. The morphology becomes inhomogeneous once the phase separation occurs in the P3HT/PS and P3HT/Ps-*co*-PHS blends. Therefore, it is likely to obtain inconsistence in the solvent diffusion region (Warburg impedance) where the straight line is originated from.

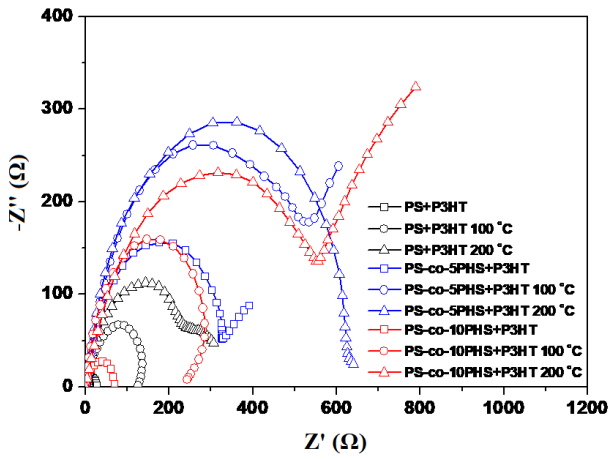


**Figure 6.** Nyquist plots of the P3HT/PS, P3HT/PS-*co*-5PHS, and P3HT/PS-*co*-10PHS coated on iron substrate in 3.5% NaCl solution.

## 4. Conclusions

Incorporation of hydroxyl group to the polystyrene enables increasing bonding strength between P3HT/PS-*co*-PHs blends and the iron substrate. Additionally, miscibility between P3HT and PS is enhanced, which also improves bonding strength of these blends and iron substrate at elevated temperature. The above-mentioned advantages make P3HT/PS-*co*-PHS blends better coating inhibitors than the P3HT/PS blend for the iron substrate. Protection efficiency levels are all above 96%.

**Supplementary Materials:** The following are available online at http://www.mdpi.com/2079-6412/8/11/383/s1, Figure S1: FT-IR study on the interaction between PS-co-PHS and $Fe_2O_3$; Figure S2: Optical microscopy photos of thermally treated PS-*co*-5PHS/P3HT blends at (a) 100 °C, 2 h and (b) 200 °C, 2 h; and PS-*co*-10PHS/P3HT blends at (c) 100 °C, 2 h and (d) 200 °C, 2 h.

**Author Contributions:** Conceptualization, P.-T.H.; Data Curation, M.-C.T., C.-R.Y. and J.-H.T.; Formal Analysis, M.-C.T. and J.-H.T.; Funding Acquisition, P.-T.H.; Investigation, J.-H.T.; Methodology, Y.-H.Y.; Project Administration, P.-T.H.; Resources, C.-R.Y.; Writing–Original Draft, M.-C.T.; Writing–Review & Editing, P.-T.H.

**Funding:** This research was funded by Fu Jen Catholic University (A0106013).

**Acknowledgments:** The authors appreciate valuable discussion with Jui-Ming Yeh.

**Conflicts of Interest:** The authors declare no conflict of interest.

## References

1. Cost of Corrosion Study. Available online: https://www.nace.org/Publications/Cost-of-Corrosion-Study/ (accessed on 14 September 2018).
2. Dariva, C.G.; Galio, A.F. Corrosion inhibitors—Principles, mechanisms and applications. In *Developments in Corrosion Protection*; Aliofkhazraei, M., Ed.; INTECH: Winchester, UK, 2014; pp. 365–379.

3. DeBerry, D.W. Modification of the electrochemical and corrosion behavior of stainless steels with an electroactive coating. *J. Electrochem. Soc.* **1985**, *132*, 1022–1026. [CrossRef]
4. Zhang, Q.; Liu, L.; Pan, C.; Li, D. Review of recent achievements in self-healing conductive materials and their applications. *J. Mater. Sci.* **2018**, *53*, 27–46. [CrossRef]
5. Taghavikish, M.; Dutta, N.K.; Choudhury, N.R. Emerging corrosion inhibitors for interfacial coating. *Coatings* **2018**, *7*, 217. [CrossRef]
6. Federica De Riccardis, M. Anticorrosion coatings based on conjugated polymers. In *Fundamentals of Conjugated Polymer Blends, Copolymers, and Composites*; Saini, P., Ed.; Scrivener Publishing LLC: Beverly, MA, USA, 2015; pp. 519–579.
7. Xiao, Y.; Ji, W.; Chang, K.; Hsu, K.; Yeh, J.; Liu, W. Sandwich-structured rGO/PVDF/PU multilayer coatings for anti-corrosion application. *RSC Adv.* **2017**, *7*, 33829–33836. [CrossRef]
8. Ji, W.; Li, C.; Yu, S.; Chen, P.; Chen, H.; Chen, R.; Hsu, C.; Yeh, J. Biomimetic electroactive polyimide with rose petal-like surface structure prepared from nanocasting technique for anticorrosive coating application. *eXpress Polym. Lett.* **2017**, *11*, 635–644. [CrossRef]
9. Chuo, T.; Yeh, J.; Liu, Y. A reactive blend of electroactive polymers exhibiting synergistic effects on self-healing and anticorrosion properties. *RSC Adv.* **2016**, *6*, 55593–55598. [CrossRef]
10. Chang, K.; Ji, W.; Li, C.; Chang, C.; Peng, Y.; Yeh, J.; Liu, W. The effect of varying carboxylic-group content in reduced graphene oxides on the anticorrosive properties of PMMA/reduced graphene oxide composites. *eXPRESS Polym. Lett.* **2014**, *8*, 908–919. [CrossRef]
11. Chang, K.; Ji, W.; Li, C.; Hsu, S.; Chuang, T.; Wei, Y.; Yeh, J.; Liu, W. Synergistic effects of hydrophobicity and gas barrier properties on the anticorrosion property of PMMA nanocomposite coatings embedded with graphene nanosheets. *Polym. Chem.* **2014**, *5*, 1049–1056. [CrossRef]
12. Yu, Y.; Yeh, J.; Jen, C.; Huang, H.; Wu, P.; Huang, C. Preparation and properties of poly(3-hexylthiophene)-clay nanocomposite materials. *J. Appl. Polym. Sci.* **2004**, *91*, 3438–3448. [CrossRef]
13. Yu, Y.; Lin, Y.; Lin, C.; Chan, C.; Huang, Y. High-performance polystyrene-/graphene-based nanocomposites with excellent anti-corrosion properties. *Polym. Chem.* **2014**, *5*, 535–550. [CrossRef]
14. Nicho, M.E.; Medrano-Baca, M.G.; León-Silva, U.; Escalante, J.; González-Rodríguez, G.; Güizado-Rodríguez, M.; Linzaga-Elizalde, I. Effect of adhesion promoter in corrosion protection of 1018 mild steel by using poly(3-hexylthiophene) coatings in 0.5 M $H_2SO_4$ solution. *Corrosion* **2011**, *67*, 105002-1–105002-12. [CrossRef]
15. Zhao, R.; Rupper, P.; Gaan, S. Recent development in phosphonic acid-based organic coatings on aluminum. *Coatings* **2017**, *7*, 133. [CrossRef]
16. Samide, A.; Eugenia Iacobescu, G.; Tutunarur, B.; Grecu, R.; Tigae, C.; Spinu, C. Inhibitory properties of neomycin thin film formed on carbon steel in sulfuric acid solution: Electrochemical and AFM investigation. *Coatings* **2017**, *7*, 181. [CrossRef]
17. Tallman, D.E.; Spinks, G.; Dominis, A.; Wallace, G.G. Electroactive conducting polymers for corrosion control. *J. Solid State Electrochem.* **2002**, *6*, 73–84. [CrossRef]
18. Ahmad, N.; MacDiarmid, A.G. Inhibition of corrosion of steels with the exploitation of conducting polymers. *Synth. Met.* **1996**, *78*, 103–110. [CrossRef]
19. Fahlman, M.; Jasty, S.; Epstein, A.J. Corrosion protection of iron/steel by emeraldine base polyaniline: An X-ray photoelectron spectroscopy study. *Synth. Met.* **1997**, *85*, 1323–1326. [CrossRef]
20. Schauer, T.; Joos, A.; Dulog, L.; Eisenbach, C.D. Protection of iron against corrosion with polyaniline primers. *Prog. Org. Coat.* **1998**, *33*, 20–27. [CrossRef]
21. Torresia, R.M.; Souzab, S.; Pereira da Silvaa, J.E.; Córdoba de Torresia, S.I. Galvanic coupling between metal substrate and polyaniline acrylic blends: Corrosion protection mechanism. *Electrochim. Acta* **2005**, *50*, 2213–2218. [CrossRef]
22. Yong, K.C. Corrosion-inhibiting behavior of epoxidized natural rubber-polyaniline dodecylbenzene-sulfonate (ENR-PANI.DBSA) blends. *Rubber Chem. Technol.* **2014**, *87*, 526–537. [CrossRef]
23. Guo, L.; Obot, I.B.; Zheng, X.; Shen, X.; Qiang, Y.; Kaya, S.; Kaya, C. Theoretical insight into an empirical rule about organic corrosion inhibitors containing nitrogen, oxygen, and sulfur atoms. *Appl. Surf. Sci.* **2017**, *406*, 301–306. [CrossRef]
24. Ren, S.; Barkey, D. Electrochemically prepared poly(3-methylthiophene) films for passivation of 430 stainless steel. *J. Electrochem. Soc.* **1992**, *139*, 1021–1026. [CrossRef]

25. Medrano-Vaca, M.G.; Gonzalez-Rodriguez, J.G.; Nicho, M.E.; Casales, M.; Salinas-Bravo, V.M. Corrosion protection of carbon steel by thin films of poly(3-alkyl thiophenes) in 0.5M $H_2SO_4$. *Electrochim. Acta* **2008**, *53*, 3500–3507. [CrossRef]
26. León-Silva, U.; Nicho, M.E. Poly(3-octylthiophene) and polystyrene blends thermally treated as coatings for corrosion protection of stainless steel 304. *J. Solid State Electrochem.* **2010**, *14*, 1487–1497. [CrossRef]
27. Hernández-Martínez, D.; León-Silva, U.; Elena Nicho, M. Corrosion protection of steel by poly(3-hexyl thiophene) polymer blends. *Anti-Corros. Methods Mater.* **2015**, *62*, 229–240. [CrossRef]